Assembly Kinetics in Binary Mixtures of Strongly Attractive Colloids

ARTICLE *in* THE JOURNAL OF PHYSICAL CHEMISTRY B · MAY 2009

Impact Factor: 3.3 · DOI: 10.1021/jp807999n · Source: PubMed

5 AUTHORS, INCLUDING:

Patrizia Andreozzi
IFOM-FIRC Institute of Molecular Oncology
20 PUBLICATIONS **316** CITATIONS
SEE PROFILE

Camillo La Mesa
Sapienza University of Rome
133 PUBLICATIONS **1,823** CITATIONS
SEE PROFILE

Francesco Sciortino
Sapienza University of Rome
408 PUBLICATIONS **17,685** CITATIONS
SEE PROFILE

Assembly Kinetics in Binary Mixtures of Strongly Attractive Colloids

Neda Ghofraniha,*,† Patrizia Andreozzi,‡,§ John Russo,†,§ Camillo La Mesa,‡,§ and Francesco Sciortino†,§

Dipartimento di Fisica, Dipartimento di Chimica, and SOFT-INFM-CNR, c/o Universita' "La Sapienza", Piazzale Aldo Moro 5, 00185 Roma, Italy

Received: September 9, 2008; Revised Manuscript Received: February 27, 2009

The early stages of aggregation kinetics in a binary mixture of asymmetric colloids, aggregating irreversibly via biotin−streptavidin bonds, are experimentally and numerically studied. Experiments are performed by DLS methods, and data are analyzed in terms of a Smoluchowski-like coagulation equation. Focus is on the case of small (S) biotin-covered particles interacting with large (L) streptavidin-covered ones. The small particles act as linkers between the large ones. The dependence of S−L and L−L aggregation rate constants on the ratio between concentration of small and large particles is investigated, to detect the concentration at which aggregation of large particles is most effective.

I. Introduction

The assembly of particles forming nano- and mesocomposites is a topic of increasing interest for material scientists and biologists.[1−10] The evolution in colloids synthesis procedures is leading to novel elementary building blocks, often characterized by anisotropic shapes,[11−14] which hold promises for the next generation of materials with ad hoc properties. In soft materials and electronic devices, the use of monodisperse and identical single component colloids is an intrinsic limit for developing systems with tunable structures.[15−17] Investigating such intriguing materials may also help understanding the intricacies inherent to the self-assembly of biological matter.[18−20]

Interesting aggregation phenomena can arise in binary, or higher order, colloid mixtures. The large number of control parameters (e.g., relative packing fractions, ratio of particles size, their relative amounts, and the material properties) offers the opportunity for a rich, polymorphic phase behavior, including the formation of different crystalline or amorphous states.[21−26] In this context, it has been recently shown that bidisperse hard spherical colloids having different sizes allow the formation of binary composites, driven by repulsive and entropic interactions.[27−31]

Coating the colloidal objects by species with high affinity, such as antigen−antibody, selectin−carbohydrate, and biotin−streptavidin/avidin, offers the possibility of selective (essentially irreversible) aggregation between distinct particles. Recently, also cDNA strands have been used to link colloids by thermoreversible specific bonds.[32−38] Biotin and streptavidin/avidin have become standard reagents to sample different reaction pathways between interacting colloid objects.[39] These techniques are commonly used to localize antigens in cells and tissues[40] and to detect biomolecules in immunoassay and DNA hybridization procedures.[41,42]

The cross-linking based on biotin−streptavidin interactions,[43−45] in particular, has been used to study aggregation in binary colloid mixtures, giving rise to clusters, chains, and interconnected network.[43−45] Indeed, in refs 43, 45, it was shown that mixing different ratios of biotin- and streptavidin-covered particles leads to the formation of disordered fractal structures. In the case that one of the two particles is significantly smaller than the other, the small particle acts as a floating bond between large ones. Hence, by controlling the relative concentration of the two species, it is possible to modulate the average number of bonds between large particles. This provides a realization of small valence systems, which have been recently investigated in their equilibrium state.[46,47]

In this Article, experimental and numerical studies on the early stages of the self-assembly kinetics[48] of bidisperse particles covered with biotin and streptavidin, respectively, are reported. In particular, a detailed study of the aggregation rates between small (S) and large (L) particles, as well as between L and L particles, mediated by small ones is performed. Number ratios of small particles (N_S) to large ones (N_L) range from 2 to 400. The aim is to detect the number ratio at which aggregation is most effective. Such a maximum is expected to arise by the balance between donor and acceptor attach sites, where donor is an attached S site while acceptor is a region of the surface of L particles not screened by attached S sites. For low N_S/N_L ratios, each L particle will only have a few floating bonds attached to it, whereas for large N_S/N_L ratios, the entire surface of L particles will be covered by S sites, preventing further adsorption stages.

Brownian dynamic simulations for the same physical parameters exploited in the experiments (concentrations, N_S/N_L, bare diffusion constants) in the limit of irreversible aggregation are also performed. Comparison between numerical and experimental results provide more details on the interactions between colloidal particles.

The rate constants estimated from dynamic light scattering experiment are found to be about 2 orders of magnitude smaller than the theoretical ones, presumably due to the presence of activation processes related to the directionality of biotin−streptavidin attraction and/or to repulsive barriers in the interaction. The experiments enlighten the presence of N_S/N_L ratios where the aggregation rate of L particles is significantly large as compared to low or high ratios. The fastest aggregation conditions are thus found.

* Corresponding author. Tel.: +39649913505. E-mail: neda.ghofraniha@roma1.infn.it.
† Dipartimento di Fisica.
‡ Dipartimento di Chimica.
§ SOFT-INFM-CNR.

10.1021/jp807999n CCC: $40.75
Published on Web 04/17/2009

II. Experiments

Materials. The system is a mixture of streptavidin-coated polystyrene particles (L) 1.0 μm in nominal diameter and biotin-coated polystyrene spheres (S) with nominal diameter 0.150 μm, purchased by Bangs Laboratories (Fishers, IN). A solution of 10 mM phosphate buffer (pH = 7.2), 20 mM NaCl, 2 mM NaN_3, and 1 wt % BSA in deionized water is prepared and filtered through a 0.22 μm Millipore filter. This solution is used to wash the spheres separately three times, and then 7.8 wt % CsCl is added to match the polystyrene particles density (1.06) and to avoid sedimentation.

Eight suspensions are prepared keeping the L-particles number density fixed to $\rho_L = 1.97 \times 10^8$ mL^{-1} (packing fraction 0.5×10^{-4}) and S-particles number density $\rho_S = \rho_L(N_S/N_L)$, with $N_S/N_L = 2$, 25, 80, 150, 200, 325, and 400. Samples S and L are sonicated separately in an ultrasonic bath at $T = 18$ °C before mixing. Each mixture is made by adding dropwise 1 mL of S particle dispersion to 1 mL of L particle ones, under gentle stirring. By mixing specific volume fractions of the two individual dispersions, binary suspensions with the desired N_S/N_L ratios are obtained. The described procedure is used for all samples, and $t_w = 0$ is the time when mixing is completed.

Experimental Methods. Dynamic light scattering (DLS) measurements are performed by a standard optical setup based on a He−Ne (wavelength $\lambda = 632.8$ nm) 8 mW laser and a photomultiplier detector in combination with an ALV-5000 logarithmic correlator. In the experiments, the scattered intensity $I(q,t)$ is measured, and the homodyne correlation function, $I_2(t) = \langle I(q,0)I(q,t)\rangle$, with q the modulus of the scattering wave vector [defined as $q = (4\pi n/\lambda)\sin(\theta/2)$], is used. n is the solvent refractive index, and the scattering angle $\theta = 90°$.

$I_1(t)$, the time correlation of the scattered electromagnetic field, is proportional to the correlation of density fluctuations. Thus, the photocorrelation data are analyzed by using the normalized correlation function $g_2(t) = I_2(t)/|I_1(t)|^2 = 1 + |I_1(t)/I_1(0)|^2$, assuming that $I_2(t) = [|I_1(0)|^2 + |I_1(t)|^2]$.[49] Because the studied samples are dilute, DLS data can be represented as a sum over the diffusional contributions of all aggregates in the system, that is:

$$g_2(t) - 1 = \left(a_0 e^{-(t/\tau_S)} + \sum_{k=1}^{\infty} a_k e^{-(t/\tau_k)}\right)^2 \qquad (1)$$

where the first term represents the dynamics of S particles, with correlation time τ_S, and the sum in the second term is extended over all L particles k-mers. Here, a_0 is the amplitude associated with the number density of S particles, and a_k is the contribution from an aggregate of L particles having size k.

To reduce the number of fit parameters, scaling relations are assumed both for the k dependence of the amplitude and for the relaxation time of clusters. For the amplitude ($a_k = a_1 k^2 \alpha^{k-1} S_k(q)$), the dependence on the squared-mass (k^2) and on the cluster structure factor ($S_k(q)$) is assumed, as well as an exponential law ($N_k \approx \exp[k \ln \alpha]$) for the cluster size distribution N_k at small k values. Such exponential law is expected for small clusters and for aggregating systems with low functionality.[50] The cluster structure factor enters in the evaluation of a_k because, in the mentioned experimental conditions, the size of the L particles (and their aggregates) is larger than the light's wavelength. Numerical analysis of the cluster structure factors[51] shows that, for $qR > 1$, $S_k(q)$ oscillates around the value $1/k$ at high q values. Hence, we have assumed that the product $k^2 S_k \approx k$. The other extreme assumption of a constant S_k does not alter significantly the results of the analysis,

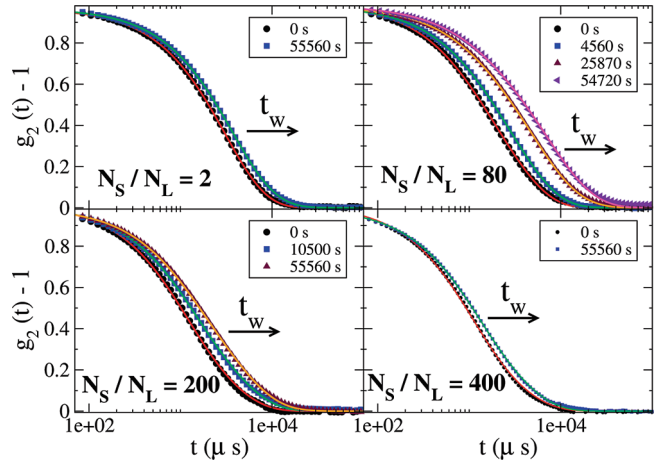

Figure 1. Normalized photon-correlation measurements for different mixtures of S and L particles during the reaction time t_w. Solid lines through data are the fitting curves obtained by using eq 2.

as discussed more in depth in the following. The cluster relaxation times scale with the hydrodynamic radii of the clusters.[51,52] Reference 53 provides a useful parametrization of $\tau_k = \tau_L b_k$ for $k > 4$ (eq 20 in ref 53), based on an analytical formula for b_k derived from the Kirkwood−Riseman theory. For clusters with $k \le 4$, the ratio $\tau_2/\tau_L = 1.38$ is taken from the literature,[54,55] and τ_3/τ_L and τ_4/τ_L are interpolated. Reference 53 also shows that for cluster sizes smaller than 100 particles there are not differences between reaction and diffusion limited cluster aggregation (RLCA, DLCA). Evaluation of the hydrodynamic radius of clusters of different sizes could also be obtained using the HYDRO++ package.[56]

Hence, DLS data are fitted with

$$g_2(t) - 1 = \left(a_0 e^{-(t/\tau_S)} + a_1 \sum_{k=1}^{\infty} \alpha^{k-1} k e^{-(t/\tau_k)}\right)^2 \qquad (2)$$

and limit the observation time of the kinetic process to values where the contribution of 100-mers to the scattering intensity is negligible (and hence the sum in eq 2 runs from 1 to 100). The fitting parameters in eq 2 are a_0, a_1, and α, while τ_S and τ_L (used to evaluate τ_k) are obtained by DLS experiments performed separately on pure S and pure L suspensions. Before being mixed, the stability of the two systems is monitored for about 2 weeks, obtaining the following diffusion coefficients: $D_L \simeq 4.8 \times 10^{-13}$ m^2/s and $D_S \simeq 2.5 \times 10^{-12}$ m^2/s (corresponding to hydrodynamic diameters $d_L \simeq 1$ μm and $d_S \simeq 200$ nm), for L and S colloids, respectively.

The described fitting procedure allows us to distinguish the contribution of small particles from large ones and their aggregates, each having different diffusion times. Other methods have been proposed,[54,57−59] where the total scattering intensity is used to estimate the coagulation rates. These methods need the knowledge of the aggregates form factors and, especially for the early stages of the coagulation, the form factor of the dimers.

Experimental Results. Figure 1 shows some measured DLS correlation functions and the related fitting curves (solid lines) for number ratios $N_S/N_L = 2$, 80, 200, and 400. Such values are taken during the first 15 h. For all N_S/N_L ratios, a detectable slowing of the correlation functions is observed, suggesting a progressive growth of the aggregates. The raw data also show rather clearly that the slowing of the dynamics is most effective for $N_S/N_L \simeq 80$. Indeed, by increasing the N_S/N_L ratio, the relaxation time of the correlation function grows more rapidly

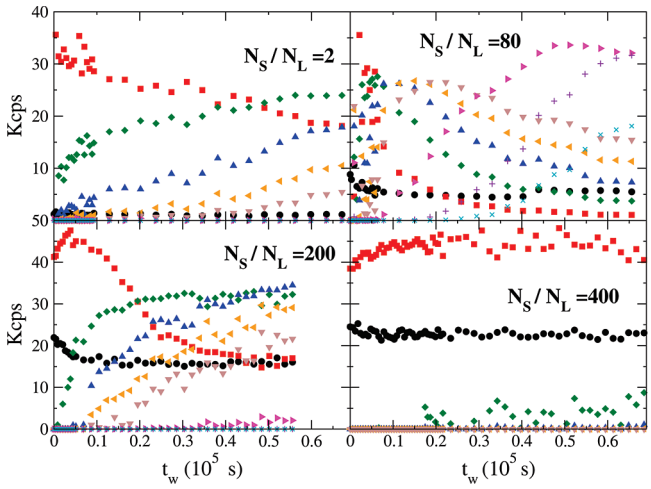

Figure 2. Light scattered intensity (kilo counts per second) of the different components in the poly disperse samples at various N_S/N_L values during the evolution time t_w (●, small particles; ■, $k = 1$; ◆, $k = 2$; ▲, $k = 3$; ◭, $k = 4$; ▼, $k = 5$; ◬, $k = 10$; +, $k = 20$; ×, $k = 30$).

with t_w until $N_S/N_L \approx 80$. For higher N_S/N_L, this growth process slows down.

Figure 2 shows the scattered intensities $I_k^s(t_w)$ of S particles ($k = 0$) and of L particles k-mers ($k \geq 1$) for the same ratios as before.The respective intensities are obtained by multiplying the fitting coefficients a_k in eq 2 by the total scattered intensity, that is, by the total number of photon counts (on the detector) per second. The time dependence of $I_k^s(t_w)$ contains information on the aggregation kinetics, because $I_k^s(t_w) = C_k\rho_k(t_w)$, with $\rho_k(t_w)$ the k-particle number density and C_k a constant term, which is the product of the scattered light intensity per k-particle times the scattering volume.

The scattered intensity evolves in time, due to progressive clustering phenomena. As in the previous figure, the case $N_S/N_L \simeq 80$ shows the most effective aggregation phenomenon, with growth of cluster sizes up to five in the explored time window, due to the fast aggregation process. In all other cases, changes in size are weaker. This is particularly evident when $N_S/N_L = 400$, where no significant decrease of the L monomers is observed. Presumably, L particles are almost completely surrounded by S ones, and L−L interactions are, thus, ineffective. For $N_S/N_L = 2$ or 80, the decrease of the population ascribed to dimers (◆ in Figure 2) with time is evident. In Figure 2, a weak maximum at small times is observed. These can be consequences of the fitting procedure, which does not account for the difference in scattering amplitude and relaxation time of L monomers with S particles attached to them. It is worth noticing that, being $\tau_L \gg \tau_S$, the contributions of the mixed system are enclosed in those pertinent to the L component in monodisperse form (i.e., $k = 1$).

Another noticeable feature is that S monomers decrease weakly with time but, except for the smallest N_S/N_L value, do not completely disappear. This is expected at large N_S/N_L ratios, due to complete coverage of L particles by S ones. However, at small N_S/N_L ratios, the number of adsorbed S particles is lower than expected. Figure 3 shows the number of S particles attached to L ones and compares the observed behavior with full adsorption predictions (dashed line).

To have quantitative information on the early stages of the kinetically controlled aggregation processes, a mean-field model for the connectivity build-up is considered.

Focus is first on the aggregation process between S and L particles. At short times, when the number of bonds is equal to

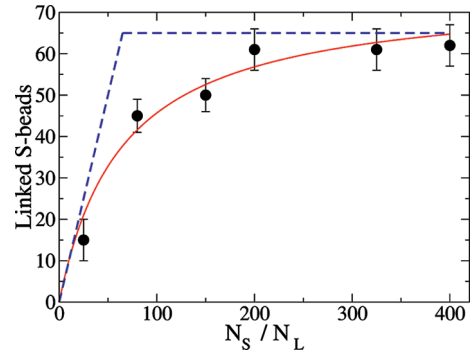

Figure 3. The number of S particles attached to L ones versus N_S/N_L ratio. The solid line is a guide to the eye. The dashed line is the expected behavior for full adsorption. The experimental points are estimated from the fraction of scattered light intensity of S particles at long times as compared to their initial value.

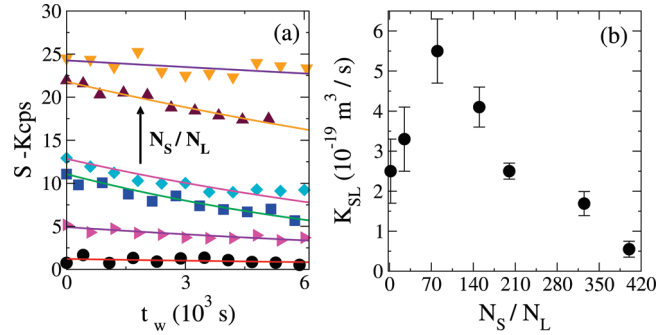

Figure 4. (a) Scattered intensities $I_0^s(t_w)$ (kilo counts per second) of S colloids while sticking to L ones at $N_S/N_L = 2$, 25, 80, 150, 200, and 400 number density ratios and the related fitting curves (solid lines through data). (b) The cross-linking rate constant K_{SL} versus the N_S/N_L ratio.

the number of dimers, the Smoluchowski coagulation equation for irreversible aggregation[60−62] simplifies to

$$\frac{d\rho_0(t_w)}{dt_w} = -K_{SL}\rho_0(0)\rho_1(0) \tag{3}$$

where $\rho_0(t_w)$ and $\rho_1(t_w)$ are the number densities of S and L particles in monomeric state at time t_w, and K_{SL} is the kernel or rate constant for the aggregation of one S particle onto an L one. The right-hand side of the above relation is evaluated at time 0 and is consistent with the approximation of short aggregation times t_w. By using the relation $\rho_0(t_w) = I_0^s(t_w)/C_0$, eq 3 reduces to

$$\frac{dI_0^s(t_w)}{dt_w} = -K_{SL}I_0^s(0)\rho_1(0) \tag{4}$$

whose solution is

$$I_0^s(t_w) = I_0^s(0)[1 - K_{SL}\rho_1(0)] \tag{5}$$

The aggregation constant K_{SL} for various N_S/N_L bonding numbers is estimated by fitting the experimental data $I_0^s(t_w)$ according to eq 5, when the starting number density, $\rho_1(0) = \rho_L$, is fixed to the experimental value (1.97×10^8 mL^{-1}). Figure 4a illustrates the scattered intensities $I_0^s(t_w)$ for different number density N_S/N_L ratios and the corresponding best-fit curves (solid lines through data). Figure 4b shows the N_S/N_L dependence of K_{SL}. Data show a pronounced maximum around $N_S/N_L \simeq 80$. The dependence on the number of small particles suggests that the approximation considering the early binary S−L aggregation

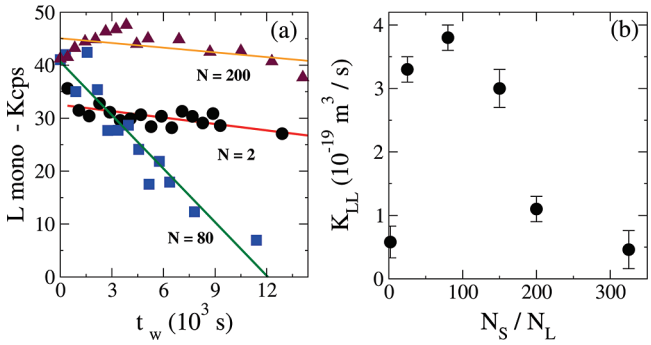

Figure 5. (a) Scattered intensities $I_1^s(t_w)$ (kilo counts per second) of L particles while forming L dimers at different N_S/N_L ratios and the fitting curves (solid lines through data). (b) The aggregation rate constant of the patchy colloids K_{LL} versus the N_S/N_L ratio.

stages is not fulfilled. Within the time window sampled experimentally, multiple encounters take place, as discussed in more detail in the comparison with simulation results.

A similar rate equation can be written for the early aggregation process of large particles:

$$\frac{d\rho_1(t_w)}{dt_w} = -K_{LL}\rho_1(0)\rho_1(0) \tag{6}$$

where K_{LL} is the kernel or rate constant for the aggregation of L particle pairs. The right-hand side of the above expression is again evaluated at time $t_w = 0$ and is consistent with the approximation of short aggregation times, t_w. By using the expression $\rho_1(t_w) = I_1^s(t_w)/C_1$, eq 6 reduces to

$$\frac{dI_1^s(t_w)}{dt_w} = -K_{LL}I_1^s(0)\rho_1(0) \tag{7}$$

whose solution is

$$I_1^s(t_w) = I_1^s(0)[1 - K_{LL}\rho_1(0)] \tag{8}$$

The corresponding results are reported in Figure 5a and b. The scattered intensities $I_1^s(t_w)$ are fitted as solid lines for different N_S/N_L ratios. At very short times, the difference in scattering amplitude and relaxation time of L particles with S ones attached is neglected. Figure 5b clearly shows that the L−L binding rate, K_{LL}, depends on N_S/N_L ratios and has a maximum at $N_S/N_L \simeq 80$.

Notice that the dependence of the reported aggregation constants on the relative concentration ratio does not change considerably by using scaling relations different from those used in eq 2. Indeed, the use of a k-independent S_k in a_k amplitudes leads to constant rates with absolute values reduced by a factor 2 as compared to those in Figure 5b, but with the same N_S/N_L dependence.

III. Theory

The system under study can be modeled as a binary mixture of particles freely diffusing and reacting on contact. This scheme is known as diffusion-limited cluster−cluster aggregation (BDLCA) and has been studied in both on-lattice[63,64] and off-lattice simulations.[65,66]

Here, Brownian dynamics simulations of a binary mixture with parameters fitting the experimental values are performed. A binary mixture of spheres with size ratio $d_L/d_S = 5.2$ (where d indicates the particles diameter) and identical ratios for the bare diffusion coefficients is studied. The particle number density is also identical to the experimental one. The simulation

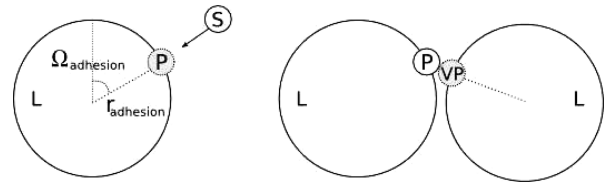

Figure 6. (a) L−S aggregation through the formation of patches on the surface of L spheres. Also depicted are the parameters $r_{adhesion}$ and $\Omega_{adhesion}$. (b) L−L aggregation. When the distance between the patch and the center of mass of colloid 2 is below d_{bond}, another patch is created (virtual patch VP). Every P−VP couple has an interaction given by V_{LS}.

runs allow one to probe the same length scale of experiments, but over times shorter than the experimental ones. The experiments suggest that the time scale of the aggregation between S and L is comparable to the one between L and L particles. Thus, the binary nature of the system is explicitly accounted for, without resorting on L particles decorated at time zero by attached S particles. At time $t = 0$, the colloid species are randomly mixed in the simulation box. As the simulation begins, colloids start diffusing. As soon as S colloids enter in contact with a L one, they stick irreversibly on the surface. Because the chemical bond between streptavidin and biotin is irreversible, the attached particles cannot diffuse on the surface of the L particles any longer. Hence, the attached S colloid is modeled as a rigid particle located on the L colloid surface (Figure 6a), which is called patch in the following. If another L particle comes sufficiently close to a patch, an irreversible bond forms between the two. To create the bond between the two colloids, the mechanism depicted in Figure 6b is used. For every newly bonded patch, a corresponding virtual patch is created (VP in the figure), and a bonding potential is switched on between the pair, establishing a stiff link between two L particles. The rationale for this choice arises from the necessity to hamper the diffusional motion of S particle on the surface of L ones, which would be inevitable if a spherical potential was used.

The interactions between the different species are described by the following potential:

$$V = V_{LL} + V_{SS} + V_{LS} \tag{9}$$

where V_{LL}, V_{SS}, and V_{LS} are the potentials between L−L, S−S, and L−S species, respectively.

The Weeks−Chandler−Anderson (WCA) potential for V_{LL} and V_{SS} is used:

$$V_{\alpha\alpha} = 4\varepsilon_\alpha\left[\left(\frac{\sigma_\alpha}{r}\right)^{12} - \left(\frac{\sigma_\alpha}{r}\right)^{6}\right] + \varepsilon_\alpha \quad r < 2^{1/6}\sigma_\alpha \quad \alpha = L, S \tag{10}$$

where r is the closest distance between the surfaces of two interacting particles (i.e., the center-to-center distance minus the sum of particles radii $(d_\alpha + d_\beta)/2$).

Small and large particles do not interact if their distance is higher than $r_{adhesion} = d_L/2$. As soon as a pair of L and S particles gets closer than $r_{adhesion}$, the location of the collision is detected, and S is replaced by a patch located at a solid angle $\Omega_{adhesion}$. Thus, $\Omega_{adhesion}$ expresses the orientation of the S species in the L body reference frame.

As discussed above, when a patch becomes closer than $d_{bond} \equiv d_S$ to the surface of an uncovered L particle, a virtual patch is created along the line connecting the given particle and the patch on the surface of another one (see Figure 6). The patch and the virtual patch interact via the FENE potential:[67]

$$V_{LS} = V_{FENE} = -\kappa(r_{max} - r_0)^2 \ln\left[1 - \left(\frac{r - r_0}{r_{max} - r_0}\right)^2\right] \quad (11)$$

which provides irreversible binding. Indeed, the FENE potential confines the two patches to stay always between $r_{min} \equiv 2r_0 - r_{max}$ and r_{max}.

Care is taken in making the simulations and the experiments numerically comparable. Because the aggregation process is irreversible, the time and length scales must be matched closely, while the energy scale is arbitrary, the bonding being irreversible. Moreover, the strength of the FENE potential is set to $\kappa = 1000$, which results in stiff bonds. The energy unit is chosen to be the parameter in the WCA potential, which ensures $\varepsilon_L = \varepsilon_S = 1$. Distances are measured in d_L units. Time is measured here in $\sigma(m/\varepsilon)^{1/2}$. Internal time $t = 1$ corresponds to a physical time $t = 0.20$ s.

The proper length scale is given by the ratio of spheres diameters, which is $d_L/d_S = 5.2$. In the simulation, the unit length is the diameter of L colloids. The WCA parameters are chosen as $\sigma_S = \sigma_L = 0.089$, $r_{max} = 0.2475$, and $r_{min} = 0.0825$. With this choice, the average distance between S spheres is the same as in the experiments. The maximum coverage is thus $N_{max} = 65$, inferred with the experimental value (Figure 3). Because in the simulations the mixture is not additive (S particles can overlap with L particles until their centers lay on L surface), the internal distance is translated in a physical distance of $d = 1.192 \times 10^{-6}$ m. In this way, when an S particle is attached on the L surface, it is at the same distance as in the experiments.

The time scale is fixed by the diffusion coefficients of the different species. Hence, their values are fixed as $D_S = 0.342$ and $D_L = 0.066$ (in internal units), so that the bare diffusion coefficient scales, as in the experiments, with the inverse of particle radius. For spheres with no-slip boundary conditions, the rotational diffusion coefficient for L colloids (D^r) is related to the translational diffusion (D^t) by the equation $D^r = 3/d_L^2 D^t$, and $D_L^r = 0.197$ (in internal units). The short-range interactions (as compared to colloids diameters) force one to use a time step of 10^{-4} in internal units.

In all simulations, the number of L spheres is $N_L = 1000$, the box size is $L = 101.55$, given the experimental volume fraction of $\phi_L = 5 \times 10^{-4}$. Number ratios N_S/N_L of 1, 3, 25, 60, 80, 100, 150, 200, and 250 are studied.

Following the analysis in section II, the Smoluchowski coagulation equations are used in the short-times limit, and eqs 3−6 are applied to extract the rate constant values as a function of N_S/N_L.

Figure 7a displays the time dependence of the number of isolated S particles and L monomers for various simulations. Figure 7b shows the corresponding aggregation constants.

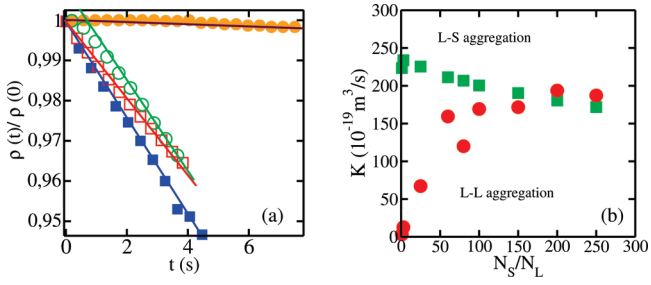

Figure 7. (a) L monomers decay for $N_S/N_L = 1$ (●) and $N_S/N_L = 250$ (○); S monomers decay for $N_S/N_L = 1$ (■) and $N_S/N_L = 250$ (□). (b) Smoluchowski rate constants for L−S aggregation (squares) and for L−L aggregation (circles). The same units as in the experiments are used.

As compared to experimental findings (see Figure 4), K_{LS} remains almost constant to $K_{LS} \cong 220 \times 10^{-19}$ m^3/s. This numerical result is expected because the kernel K_{LS} does not depend on the concentration of the two species. This value coincides with the Smoluchowski Brownian dimer formation rate, $K_{LS}^{Brownian}$, which can be written[60] as a product of the relative diffusion constants and of the aggregation distance. For the present system, $K_{LS}^{Brownian} = 4\pi(D_L + D_S)d_L \simeq 220 \times 10^{-19}$ m^3/s.

As the ratio N_S/N_L increases, a very small decrease of K_{LS} is observed. It is associated with the onset of a nonlinear dependence in the time evolution of the small particles number density, suggesting that, on increasing N_S, the short-time approximation of eq 3 breaks down.

Figure 7a and b also displays the time dependence of L monomers and the associated K_{LL} values. The aggregation rate grows for $N_S/N_L \lesssim 150$, after which it remains almost constant.

IV. Discussion and Conclusions

To study the irreversible aggregation of a binary mixture of particles, coated with biotin and streptavidin, respectively, DLS measurements are reported. Focus was on two processes: the bonding between large (L) streptavidin-covered and small (S) biotin-covered particles, and the aggregation of L particles, held together via the bridging of S particles.

The observed rate constants of L−S and L−L stages are comparable, meaning that both processes occur on the same time scales, despite the different size ratios. The estimated values of the constants for L−S and L−L aggregation are shown in Figures 4b and 5b. These values are far below the theoretical predictions for irreversibly aggregating Brownian particles (interacting via a deep short-ranged attractive potential) by almost 2 orders of magnitude. This difference could be related to the particular behavior of biotin−streptavidin interaction when attached to substrates. As discussed in refs 68, 69, the biotin−streptavidin rate constant reduces dramatically when the proteins are constrained onto surfaces. Because the interaction is strongly orientation dependent, the binding onto surfaces limits greatly the ability of the proteins to form bonds. The present results strongly suggest that the L−S aggregation is not only controlled by diffusion and that biotin−streptavidin reaction requires an activation process, which could be related to an entropic barrier associated with the directionality and geometric specificity of the interaction, or to a repulsive energetic barrier in the interaction potential. Such hypothesis is also consistent with the significant fraction of small particles that remains unattached even after long observation times, as shown in Figure 3. To confirm that the reduction of reaction rates does not depend on the specific composition of the system, Brownian dynamics simulations of irreversibly aggregating spherically interacting particles are performed. The simulated particles have size ratios, diffusion coefficients, and relative compositions equal to the experimental ones. For this simulated system, the expected Brownian reaction rate ($\sim 220 \times 10^{-19}$ m^3/s) is indeed recovered, confirming that entropic or energetic barriers must be present in the real system.

A significant N_S/N_L dependence of the rate constants experimentally measured is observed: both L−S and L−L aggregation constants show a peak at $N_S/N_L \simeq 80$ (Figures 4b and 5b), suggesting that in the experimentally accessible time window a coupling between the two processes is present. Simulations confirm these hypotheses. Indeed, in the simulation the early time of the aggregation is explored, confirming that in this initial time window no significant coupling of the rate constants is

found (Figure 7). As the number of S particles increases, only a slight decrease is observed, due to the repulsion between S particles in solution and those bound to L ones. This repulsion causes the slowing of the reaction. In the experiments (Figure 4), a decay of the rate constant is observed only for high N_S/N_L values, but it is preceded by an increase of the same constant value, which reaches a maximum at $N_S/N_L \simeq 80$.

The L−L aggregation process results are shown in Figure 5 (experiments) and in Figure 7 (simulations). Simulations predict a rapid increase of the rate constant with growing N_S/N_L, due to the increasing number of sticking S particles binding onto L ones. The experiments show that this is, in fact, the case and that the rate constants increase until $N_S/N_L \simeq 80$. Thereafter, they rapidly decrease, because of the saturation of S particles on L surfaces at high N_S/N_L values. Unfortunately, the rapid decrease cannot be observed in the simulations, because the accessible time scale allows one to probe a time window in which only a limited number of S particles are attached onto L ones. The average coverage from simulations is always less than 10 particles, far below the estimated saturation value (∼65). Conversely, the experiments explore the decay of L monomers in the time region where the number of attached S particles is close to maximum coverage. The rapid decrease is a consequence of the repulsion of highly S-covered L particles. The peak position for the L−L rate constant ($N_S/N_L \simeq 80$) corresponds to an average number of ≃40 S particles attached to an L, because most S particles are still in solution as monomers. A possible explanation of excess of S particles in solution relays on the fact that L−L aggregates expose less surface to the binding with S particles than do single L ones. This effect takes place because the L−L aggregation occurs on the same time scale as the L−S aggregation.

In summary, the ratio N_S/N_L provides an efficient way for controlling the average connectivity and the aggregation rate,[70] providing a method for controlling the morphology of the aggregates by modulating the number of interparticle bonds.[43,45] It shows that the average number of L−L bonds does not correspond to the number of S particles, because some of them remain in solution as single species. A comparison between experimental and numerical results is presented as a method for clarifying the physics behind the aggregation process.

References and Notes

(1) Yi, G.; Manoharan, V. N.; Michel, E.; Elsesser, M. T.; Yang, S.; Pine, D. J. *Adv. Mater.* **2004**, *16*, 1204.
(2) Liddell, C. M.; Summers, C. J. *Adv. Mater.* **2003**, *15*, 1715.
(3) Manoharan, V. N.; Elsesser, M. T.; Pine, D. J. *Science* **2003**, *301*, 483.
(4) Mirkin, C. A.; Letsinger, R. L.; Mucic, R. C.; Storhoff, J. J. *Nature (London)* **1996**, *382*, 607.
(5) Glotzer, S. C. *Science* **2004**, *306*, 419.
(6) Mladek, B. M.; Kahl, G.; Likos, C. N. *Phys. Rev. Lett.* **2008**, *100*, 028301.
(7) Jackson, A. M.; Myerson, J. W.; Stellacci, F. *Nat. Mater.* **2004**, *3*, 330.
(8) Whitesides, G. M.; Boncheva, M. *Proc. Natl. Acad. Sci. U.S.A.* **2002**, *99*, 4769.
(9) Starr, F. W.; Douglas, J. F.; Glotzer, S. C. *J. Chem. Phys.* **2003**, *119*, 1777.
(10) Starr, F. W.; Sciortino, F. *J. Phys.: Condens. Matter* **2006**, *18*, L347.
(11) Zhang, Z.; Horsch, M. A.; Lamm, M. H.; Glotzer, S. C. *Nano Lett.* **2003**, *3*, 1341.
(12) Glotzer, S. C.; Solomon, M. J. *Nat. Mater.* **2007**, *6*, 557.
(13) Zhao, K.; Mason, T. G. *Phys. Rev. Lett.* **2007**, *99*, 268301.
(14) Zhang, Z.; Keys, A. S.; Chen, T.; Glotzer, S. C. *Langmuir* **2005**, *21*, 1154.
(15) Wang, H.; Lu, Y. F. *J. Appl. Phys.* **2008**, *103*, 3113.
(16) Tang, Z.; Zhang, Z.; Wang, Y.; Glotzer, S. C.; Kotov, N. A. *Science* **2006**, *314*, 274.
(17) Maldovan, M.; Thomas, E. L. *Nat. Mater.* **2004**, *3*, 593.
(18) Šiber, A.; Podgornik, R. *Phys. Rev. E* **2007**, *76*, 061906.
(19) Hu, T.; Shklovskii, B. I. *Phys. Rev. E* **2007**, *75*, 051901.
(20) Fuechslin, R. M.; Maeke, T.; Tangen, U.; McCaskill, J. S. *arXiv e-prints* **2007**, 705.
(21) Harris, N.; Ford, M. J.; Cortie, M. B.; McDonagh, A. M. *Nanotechnology* **2007**, *18*, J5301.
(22) Zhang, J.; Liu, H.; Wang, Z.; Ming, N. *J. Appl. Phys.* **2008**, *103*, 3517.
(23) Shih, W. Y.; Shih, W.-H.; Aksay, I. A. *J. Chem. Phys.* **1989**, *90*, 4506.
(24) Bartlett, P.; Campbell, A. I. *Phys. Rev. Lett.* **2005**, *95*, 128302.
(25) Martin, S.; Bryant, G.; van Megen, W. *Phys. Rev. E* **2005**, *71*, 021404.
(26) Schofield, A. B.; Pusey, P. N.; Radcliffe, P. *Phys. Rev. E* **2005**, *72*, 031407.
(27) Baumgartl, J.; Dullens, R. P. A.; Dijkstra, M.; Roth, R.; Bechinger, C. *Phys. Rev. Lett.* **2007**, *98*, 198303.
(28) Wong, A. C. T.; Yu, K. W. *Physica A* **2002**, *312*, 50.
(29) Hennequin, Y.; Pollard, M.; van Duijneveldt, J. S. *J. Chem. Phys.* **2004**, *120*, 1097.
(30) Méndez-Alcaraz, J. M.; D'Aguanno, B.; Klein, R. *Physica A* **1991**, *178*, 421.
(31) Bartlett, P.; Pusey, P. N. *Physica A* **1993**, *194*, 415.
(32) Biancaniello, P. L.; Kim, A. J.; Crocker, J. C. *Phys. Rev. Lett.* **2005**, *94*, 058302.
(33) Mirkin, C. A.; Letsinger, R. L.; Mucic, R. C.; Storhoffand, J. J. *Nature (London)* **1996**, *382*, 607.
(34) Harris, N. C.; Kiang, C.-H. *Phys. Rev. Lett.* **2005**, *95*, 046101.
(35) Sánchez-Pomales, G.; Rivera-Vélez, N. E.; Cabrera, C. R. *J. Phys. Conf. Ser.* **2007**, *61*, 1017.
(36) Yao, H.; Yi, C.; Tzang, C.-H.; Zhu, J.; Yang, M. *Nanotechnology* **2007**, *18*, 5102.
(37) Talanquer, V. *J. Chem. Phys.* **2006**, *125*, 4701.
(38) Geerts, N.; Frenkel, D.; Eiser, E.; Schmatko, T.; Bozorgui, B.; Poon, W. C. K. *Soft Matter* **2007**, *3*, 703.
(39) Bayer, E. A.; Wilchek, M. *Anal. Biochem.* **1988**, *171*, 1.
(40) Holmes, K. V.; Armstrong, R.; Friedrich, V. L., Jr.; Dubois-Dalcq, M. *J. Cell Biol.* **1990**, *111*, 1183.
(41) Davis, L. M.; Fan, Y.; Shows, T. B. *Proc. Natl. Acad. Sci. U.S.A.* **1990**, *87*, 6223.
(42) Singer, R. H.; Lawrence, J. B.; McNeil, J. A. *Science* **1990**, *249*, 249.
(43) Hiddessen, A. L.; Rodgers, S. D.; Weitz, D. A.; Hammer, D. A. *Langmuir* **2000**, *16*, 9744.
(44) Milam, V. T.; Hiddessen, A. L.; Rodgers, S. D.; Crocker, J. C. *Langmuir* **2003**, *19*, 10317.
(45) Hiddessen, A. L.; Weitz, D. A.; Hammer, D. A. *Langmuir* **2004**, *20*, 6788.
(46) Bianchi, E.; Tartaglia, P.; La Nave, E.; Sciortino, F. *J. Phys. Chem. B* **2007**, *111*, 11765.
(47) Bianchi, E.; Largo, J.; Tartaglia, P.; Zaccarelli, E.; Sciortino, F. *Phys. Rev. Lett.* **2006**, *97*, 168301.
(48) Sciortino, F.; De Michele, C.; Douglas, J. F. *J. Phys.: Condens. Matter* **2008**, *20*, 5101.
(49) Berne, B. J.; Pecora, R. *Dynamic Light Scattering*; John Wiley and Sons: New York, 1976.
(50) Sciortino, F.; Bianchi, E.; Douglas, J. F.; Tartaglia, P. *J. Chem. Phys.* **2007**, *126*, 4903.
(51) Lattuada, M.; Hua, W. U.; Morbidelli, M. *J. Colloid Interface Sci.* **2003**, *268*, 106.
(52) Sandk, M. *Adv. Colloid Interface Sci.* **2005**, *113*, 65.
(53) Lattuada, M.; Hua, W. U.; Morbidelli, M. *J. Colloid Interface Sci.* **2003**, *268*, 96.
(54) Yu, W. L.; Matijevic, E.; Borkovec, M. *Langmuir* **2002**, *18*, 7853.
(55) Holthoff, H.; Egelhaaf, S. U.; Borkovec, M.; Schurtenberger, P.; Sticher, H. *Langmuir* **1996**, *12*, 5541.
(56) Garcia de la Torre, J.; del Rio, G.; Ortega, A. *J. Phys. Chem. B* **2007**, *111*, 955.
(57) Ryde, N.; Matijevic, E. *J. Chem. Soc., Faraday Trans.* **1994**, *90*, 167.
(58) Wei, L.; Kobayashi, M.; Skarba, M.; Changdao, M.; Galletto, P.; Borkovec, M. *Langmuir* **2006**, *22*, 1038.
(59) Lopez-Lopez, J. M.; Schimtt, A.; Moncho-Jorda, A.; Hidalgo-Alvarez, A. *Soft Matter* **2006**, *2*, 1025.
(60) Russel, W. B.; Saville, D. A.; Schowalte, W. R. *Colloidal Dispersions*; Cambridge University Press: Cambridge, 1991.
(61) Galina, H.; Lechowicz, J. B. *Adv. Polym. Sci.* **1998**, *137*, 136.
(62) Galina, H. *Europhys. Lett.* **1987**, *3*, 1155.
(63) Meakin, P.; Djordjević, Z. B. *J. Colloid Interface Sci.* **1986**, *19*, 2137.
(64) AlSunaidi, A.; Lach-hab, M.; Gonzáles, A. E.; Blaisten-Barojas, E. *Phys. Rev. E* **2000**, *61*, 550.

(65) Puertas, A. M.; Fernández-Barbero, A.; de las Nieves, F. J. *J. Chem. Phys.* **2001**, *115*, 5662.
(66) López-López, J. M.; Moncho-Jordá, A.; Schmitt, A.; Hidalgo-Álvarez, R. *Phys. Rev. E* **2005**, *82*, 031401.
(67) Kremer, K.; Grest, G. S. *J. Phys.: Condens. Matter* **1990**, *2*, 295.
(68) Weiss, R.; Caldwell, K. D.; Huang, S. C.; Stump, M. D. *Anal. Biochem.* **1996**, *237*, 115.
(69) Cohen-Tannoudji, L.; Bertrand, E.; Baudry, J.; Robic, C.; Goubault, C.; Pellissier, M.; Johner, A.; Thalmann, F.; Lee, N. K.; Marques, C. M.; Bibette, J. *Phys. Rev. Lett.* **2008**, *100*, 108301.
(70) Moncho-Jordá, A.; Odriozola, G.; Tirado-Miranda, M.; Schmitt, A.; Hidalgo-Álvarez, R. *Phys. Rev. E* **2003**, *68*, 011404.

JP807999N